JOURNAL OF GEOPHYSICAL RESEARCH, VOL. 99, NO. D2, PAGES 3685–3698, FEBRUARY 20, 1994

11-μm emissivities and droplet radii for marine stratocumulus

Gang Luo,[1] Xijian Lin, and James A. Coakley, Jr.
College of Oceanic and Atmospheric Sciences, Oregon State University, Corvallis

Abstract. The results of a new multispectral infrared retrieval scheme for obtaining fractional cloud cover and 11-μm emissivity are compared with those of the spatial coherence method which obtains fractional cloud cover assuming that the clouds are opaque at infrared wavelengths. Both methods are applied to 4-km NOAA advanced very high resolution radiometer global area coverage data for 250-km-scale regions containing single-layered marine stratocumulus off the coast of South America. The average 11-μm emissivity for low-level clouds is found to be between 0.70 and 0.85. The low emissivity is evidently due to the thinning of clouds at their edges. Semitransparent cloud edges evidently make up a substantial portion of the area covered by such clouds. This result indicates that cloud cover obtained using the spatial coherence method is underestimated by 0.1 to 0.2, as has been claimed in a previous study. The fractional cloud cover for the ensemble of 250-km-scale regions studied here increased slightly from 0.60 for daytime observations to 0.63 for nighttime observations. The 11-μm emissivity also increased slightly, but about half of the increase was related to the increase in cloud cover and a decrease in the relative area covered by cloud edge material. Presumably, the other half was due to an increase in cloud liquid water. Cloud height showed no significant change. The average effective droplet radius increased from 9.3 μm for daytime observations to 10.2 μm at night.

1. Introduction

The spatial coherence method for retrieving cloud properties from satellite imagery data was designed to allow for clouds that failed to fill the imager's field of view [*Coakley and Bretherton*, 1982]. Provided the cloud was opaque at the infrared wavelength at which the retrieval was undertaken and was in a well-defined layer, the fractional cloud cover for any imager pixel could be obtained to within a range of uncertainty that could also be determined. Through the relationship between emission at 3.7 and 11 μm, two wavelengths for which the optical properties of ice and water differ and for which the sensitivity of blackbody emission to temperature is quite different, the validity of the assumptions concerning cloud layering and opacity could be examined [*Coakley*, 1983; *Coakley and Davies*, 1986]. A cursory examination of emission at 3.7 and 11 μm for single-layered cloud systems revealed that such clouds often appeared to be opaque but of course were not always so [*Molnar and Coakley*, 1985].

Wielicki and Parker [1992] applied the spatial coherence method to ultra-high-resolution (114 m) Landsat observations and compared the retrieved fractional cloud cover with that obtained with a threshold method for which the uncertainty in cloud cover could be measured. The fractional cloud cover obtained with the spatial coherence method was typically 0.18 below that obtained with the results of a control threshold retrieval for which the typical uncertainty in the cloud cover was estimated to be less than 0.05. The bias could not be explained either by the uncertainty estimated in the threshold results or by that derived from the spatial coherence method. Wielicki and Parker further demonstrated that the bias was probably due to the edges of clouds becoming semitransparent at 11 μm. Evidently, the fractional cloud cover reported in a spatial coherence retrieval was not the actual area covered but an emissivity-weighted area.

The Wielicki and Parker study, however, was constrained to a limited sample of Landsat images (24 images, each 58.4 km on a side). To determine how extensive the bias to spatial coherence results might be, we have used a new multispectral infrared retrieval method [*Lin and Coakley*, 1993] to obtain the 11-μm emissivities of single-layered marine stratocumulus for an extensive ensemble of $(250\text{-km})^2$ regions off the coast of South America. Over a thousand such regions have been included in this study. Both daytime and nighttime observations were analyzed. We find that Wielicki and Parker were correct. Owing to the semitransparency of the edges of marine stratocumulus, the spatial coherence method underestimates fractional cloud cover on the $(250\text{-km})^2$ scale by about 0.15.

2. Theory

Lin and Coakley [1993] have described a retrieval scheme that obtains the distribution of pixel-scale fractional cloud cover and liquid/ice water paths from emissions at 11 and 12 μm observed with the NOAA advanced very high resolution radiometer (AVHRR). The algorithm utilizes differences in the optical properties of water and ice at the different wavelengths to analyze clouds that are semitransparent at infrared wavelengths. As part of the retrieval procedure, an effective radius for the cloud particles is also obtained. The

[1]Now at UCAR Visiting Scientist Program, NOAA National Environmental Satellite Data and Information Service, Camp Springs, Maryland.

Copyright 1994 by the American Geophysical Union.

Paper number 93JD02462.
0148-0227/94/93JD-02462$05.00

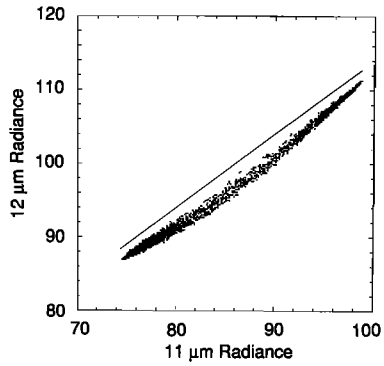

Figure 1. Observed 11- and 12-μm radiances (mW m^{-2} sr^{-1} cm) for a (250-km)^2 region containing a single-layered stratocumulus cloud system over the Pacific Ocean off the coast of South America. Each point represents a (4-km)^2 portion of the region on April 9, 1985, at 2100 UT centered at 29°S, 89°W. The line in the figure is straight and is meant to serve as a reference against which to compare the curvature of the relationship between 11- and 12-μm radiance pairs.

method is strictly applicable to single-layered systems of broken clouds, of which marine stratocumulus are the obvious example.

In the multispectral infrared retrieval, radiances at 11 and 12 μm observed in a pixel containing a single cloud layer are taken to be given by

$$I_i = (1 - A_c)I_{si} + A_c(\varepsilon_i I_{ci} + t_i I_{si}) \quad (1)$$

where A_c is the fraction of the pixel covered by cloud, ε_i is the emissivity of the cloud for the wavelengths associated with channel i, t_i is the transmissivity of the cloud, I_{ci} is the emission that would be obtained for overcast regions were the clouds to emit as blackbodies at the temperature associated with the cloud layer, and I_{si} is the emission associated with the cloud-free background. For emission at 11 and 12 μm the emissivity is taken to be unity when the clouds become opaque. Consequently, I_{ci} is the emission associated with regions overcast by opaque cloud. For a moderately sized region (~50- to 250-km scale) containing a single layer of broken clouds, the pixel-scale 11- and 12-μm emitted radiances will in general form a two-dimensional distribution as shown in Figure 1. The line in the figure is straight and provides a reference against which to compare the curvature of the 11- and 12-μm radiance relationships. Figure 2 shows the results of radiative transfer calculations of thermal emission for a single-layered cloud system. The results shown in Figure 2 are obtained using (1), with Mie theory used to obtain the single scattering properties of the cloud droplets and the Eddington approximation [*Goody and Yung*, 1989] used to obtain the emissivities and transmissivities of clouds with various amounts of liquid water. The use of the Eddington approximation for this study will be examined in section 5. As is discussed later, values for the cloud-free emission I_{si} and for the overcast, opaque cloud emission I_{ci} are obtained from the observed radiances and thus contain effects due to the radiatively active components of the cloud-free atmosphere.

The distribution of radiance pairs emitted by a single-layered cloud system will, depending on the distribution of fractional cloud cover and liquid/ice water paths within the region, fill the "envelope" formed by the bispectral curves shown in Figure 2. The envelope is determined on one side by a straight line. A linear relationship between radiances at 11 and 12 μm could indicate that the clouds in the layer are opaque. The straight line is obtained from (1) by taking the limit of optically thick cloud, that is, $t_i = 0$ and $\varepsilon_i = \varepsilon_{i\max}$, a constant, maximum value, which for 11 and 12 μm is taken to be unity. In this limit, (1) can be used to show that since radiances at 11 and 12 μm depend linearly on the fractional cloud cover, they also depend linearly on each other. But as Lin and Coakley point out, a linear relationship could also indicate that the droplets are sufficiently large that their absorption and extinction cross sections are identical at the two wavelengths despite the differences in the bulk optical properties of water. This limit for 11- and 12-μm radiances is obtained when the droplet radius reaches about 20 μm, which is larger than radii often found in marine stratocumulus [*Nakajima et al.*, 1991].

The nonlinear curve shown in Figure 2 represents pixels that are overcast by clouds associated with the layer that are semitransparent. The curve is obtained from (1) by setting $A_c = 1$ and calculating 11- and 12-μm radiances for various liquid/ice water column amounts. The column amounts along the curve vary from zero at the cloud-free end where the curve meets the straight line (high 11- and 12-μm radiances) to amounts sufficient for the cloud to be opaque at the other intersection of the curved and straight lines. As discussed by Lin and Coakley, the area of the 11- to 12-μm radiance domain covered by the radiance pairs associated with an ensemble of pixels is governed by droplet size. Small droplets yield large areas; large droplets yield small areas. As noted above, for radiances at 11 and 12 μm, the curve and straight line converge (zero area) when the droplet radii exceed approximately 20 μm.

Cloud properties are retrieved from the distribution of pixel-scale radiances for a region by fitting the results of radiative transfer calculations using (1) to the distribution of observed radiances. For the radiative transfer calculations, the emission associated with cloud-free pixels I_{si} and the emission associated with pixels overcast by opaque cloud $\varepsilon_{i\max}I_{ci}$ with $\varepsilon_{i\max} = 1$ are obtained from the spatial coher-

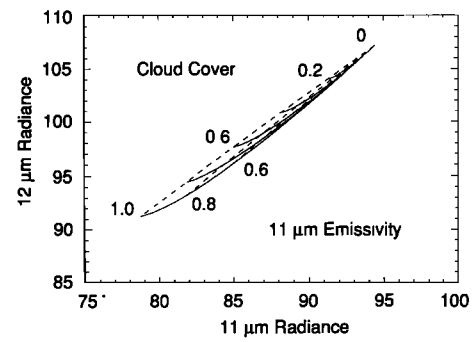

Figure 2. The 11- and 12-μm radiances (mW m^{-2} sr^{-1} cm) calculated for a single-layered cloud system. The dashed curves give the radiances for fixed values of the 11-μm emissivity. The solid curves give radiances for fixed fractional cloud cover. The values above the envelope indicate the fractional cloud cover, and those below the envelope indicate the 11-μm emissivity. The effective droplet radius for these calculations was 5.5 μm.

ence method [*Coakley and Baldwin*, 1984]. A single "effective droplet radius" is assumed for all the clouds in the region, and the effective radius is adjusted to obtain a satisfactory fit to the nonlinear envelope of the observed 11- to 12-μm radiance distribution. Once a suitable fit has been obtained, the distributions of fractional cloud cover and 11-μm emissivities are derived on the basis of interpretation provided by the radiative transfer calculations. Figure 2 shows how the 11- and 12-μm radiance pairs for individual pixels would divide the pixels according to their fractional cloud cover and 11-μm emissivity. This retrieval scheme is similar in principle to schemes described by *Platt* [1983] and *Arking and Childs* [1985].

The retrieved effective droplet radius should be taken only as an index of droplet size. In situ as well as remotely sensed observations of droplet sizes for marine stratocumulus indicate that droplet sizes change dramatically within typical cloud cells [*Nakajima et al.*, 1991]. At best, the effective radius retrieved here should be used only to indicate whether the droplets are relatively large or small on a regional scale. The results presented in section 5 show that this index for 250-km-scale regions exhibits the range of values often found for droplet radii in marine stratocumulus.

It should also be noted that the retrieval method is rather arbitrary. For example, a single droplet radius instead of a droplet size distribution is used to represent droplet sizes. Use of a realistic droplet size distribution in the retrieval would simply alter the definition of the retrieved droplet radius. Tests employing a log-normal droplet size distribution, like that employed by *Nakajima and King* [1990], indicate that the retrieved effective radius is near the value given by the ratio of the volume to area moments of the droplet size distribution. Whether or not the effective radius is linked to a parameter in a size distribution, it would remain an index for distinguishing between regional-scale cloud systems with distinctly different droplet sizes. Consequently, there appears to be no advantage in using a size distribution instead of the single-size model used here.

In addition, one possible scenario is that all of the points in Figure 1 that are not associated with pixels identified as being cloud-free could be interpreted as being due to overcast pixels, as is commonly done in threshold methods [*Minnis and Harrison*, 1984; *Rossow et al.*, 1985]. Then, the

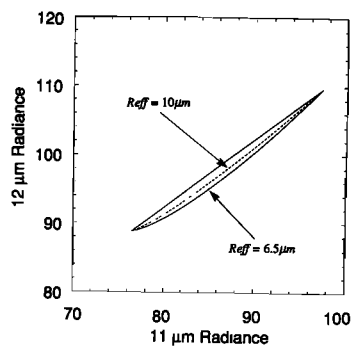

Figure 3. The 11- and 12-μm radiances (mW m^{-2} sr^{-1} cm) calculated for a single-layered cloud system. The solid curve gives radiances for pixels overcast by semitransparent clouds having a droplet radius of 6.5 μm. The dashed curve gives radiances for pixels overcast by semitransparent clouds having a droplet radius of 10 μm.

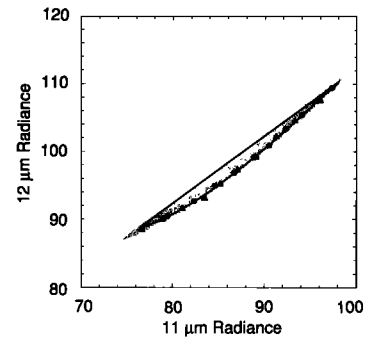

Figure 4. Calculated radiances (mW m^{-2} sr^{-1} cm) fit to the observations shown in Figure 1. The endpoints of the envelope were determined through spatial coherence analysis. The fifth percentiles of the observed 12-μm radiances in each 11-μm radiance bin are indicated by triangles. The 12-μm radiances on the lowest curve of the envelope were calculated using the procedure described in the text. The 95th percentiles of the observed 11-μm radiances in each 12-μm radiance bin are indicated by large dots.

variation in 11- and 12-μm radiances would be interpreted as being due to variations in liquid/ice water path and droplet size. We do not adopt this interpretation, simply because it is improbable that a 250-km region would have an extensive layer of marine stratocumulus but be devoid of opaque clouds at the 4- to 8-km scale. We suspect that pixels with radiances falling near the straight line envelope in the 11- to 12-μm radiance domain are indeed due to fields of view that are partly covered by opaque clouds as opposed to being overcast by semitransparent clouds that have large droplets. This inference is based on the common occurrence of a linear relationship between 3.7- and 11-μm emissions for nighttime observations [*Coakley*, 1983; *Molnar and Coakley*, 1985; *Coakley and Davies*, 1986]. For 3.7- and 11-μm radiances to be linearly related as a result of emission by semitransparent clouds, the effective droplet radius would have to exceed 60 μm [*Lin and Coakley*, 1993], a value that vastly exceeds the 5- to 20-μm radii typically found in marine stratocumulus [*Nakajima et al.*, 1991].

As was noted by Lin and Coakley, the retrieval scheme used here suffers from ambiguities. An example is illustrated schematically in Figure 3. The figure shows two curved lines, one giving overcast radiances for a small droplet radius (solid curve) and a second giving overcast radiances for a larger droplet radius (dashed curve). In the scheme used here, the retrieved effective radius will be set equal to the smaller value, as the curve associated with the smaller droplet radius would encompass the lower extreme occupied by the pixel-scale radiance pairs in the 11- to 12-μm radiance domain. Nevertheless, should some of the clouds in the region contain the larger droplet radius, then they would be interpreted as being associated with broken clouds. If some of the pixels were overcast so that their 11- and 12-μm radiance pairs followed the dashed curve in Figure 3, then for these pixels the retrieved cloud cover would underestimate the actual cover and the retrieved emissivity would overestimate the actual emissivity.

Likewise, the pixels having radiance pairs that fell near the straight line would be taken to contain opaque, broken clouds. If the clouds were indeed opaque, they would

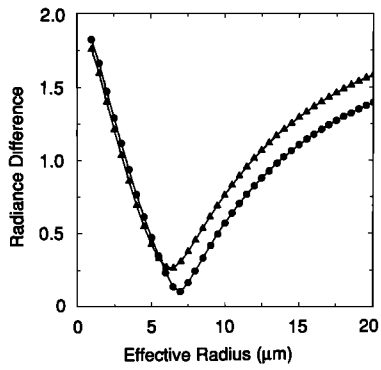

Figure 5. RMS differences between observed and calculated radiances (mW m^{-2} sr^{-1} cm) and effective droplet radius (μm). Dots are for the fifth percentiles of the observed 12-μm radiances in each 11-μm radiance bin. Triangles are for the 95th percentiles of the observed 11-μm radiances in each 12-μm radiance bin.

populate this line regardless of droplet size. It is conceivable that clouds having droplets smaller than that given by the lower boundary associated with semitransparent cloud could produce radiances along the straight line. Consequently, the lower boundary need not represent the smallest droplets associated with the clouds.

Finally, as was noted above, semitransparent clouds having large droplets ($R_{\text{eff}} > 20$ μm) would also produce radiance pairs along the straight line. Such clouds can have any emissivity and cloud cover provided the product of their emissivity and fractional cloud cover equals that obtained for the opaque cloud model, that is, $\varepsilon' A'_c = A_c$. Consequently, for the pixels containing semitransparent clouds having large droplet radii, the emissivity would again be overestimated by the current procedure, and the cloud cover would be underestimated.

The degree of bias in the derived 11-μm emissivity and fractional cloud cover associated with the current method is unknown. It appears, however, that provided the single-layer approximation is realistic, knowledge of the effective droplet radius associated with the individual pixels may remove the bias. Such knowledge may come from simultaneous observations for the other spectral channels (0.63 and 3.7 μm) available from AVHRR observations. Unfortunately, retrievals using 3.7-μm radiances require corrections for absorption and emission by the other radiatively active components of the atmosphere in order to deduce the 3.7-μm emissivity associated with opaque clouds, which is itself a function of droplet size. This emissivity is required in order to predict the emission associated with opaque cloud on the basis of the cloud emission temperature, which in turn might be obtained from emission at 11 and 12 μm after corrections have been made for absorption and emission at these wavelengths by the gases in the atmosphere (primarily water vapor). Here, no such corrections are required, because the emissivities for opaque clouds at 11 and 12 μm are taken to be unity, and the radiances associated with overcast opaque clouds I_c and cloud-free regions I_s are observed and thus include effects due to the other radiatively active components of the atmosphere. *Minnis et al.* [1992] succeeded in retrieving the effective droplet radius from visible and infrared imagery data combined with liquid water paths obtained from a surface-based microwave radiometer. In view of the ambiguities inherent in the current approach, comparison of retrievals using the current method with those based on visible and 11-μm radiances are clearly warranted.

3. Retrieval Method

For the current retrievals the spatial coherence method was used to obtain the emission associated with the cloud-free background and with regions that were overcast by opaque cloud [*Coakley and Baldwin*, 1984]. Figure 4 shows the calculated envelope and observed 11- and 12-μm radiances for a 250-km region (64 × 64 scan line × scan spot array of 4-km pixels) of the Pacific Ocean off the coast of South America that contains a single-layer, broken-cloud system, as was indicated by the results of spatial coherence analysis. The curve associated with overcast, semitransparent cloud was obtained in the following manner. The range of 11-μm radiances between the emission associated with cloud-free and overcast pixels as deduced by the spatial coherence method was divided into 10 equal intervals. If the clouds were opaque, each of the 10 equally spaced 11-μm radiance intervals would be associated with each 0.1 increment in fractional cloud cover. Semitransparent clouds give rise to the curve at the lower part of the two dimensional diagram depicted in Figures 2 and 4. To fit these curves, the pixel having the 12-μm radiance nearest the fifth percentile of the 12-μm radiances within each 11-μm radiance interval was identified. These pixels are identified by the triangles in Figure 4. A group of curves for overcast semitransparent clouds was calculated using the radiative transfer model employing the Eddington approximation and single effective droplet radius. The curves were for effective droplet radii

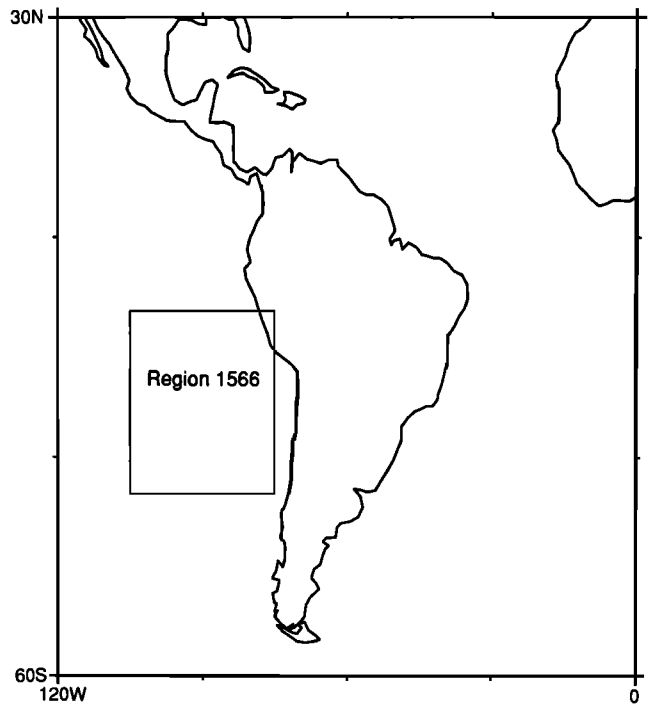

Figure 6. The location of ERBE V-5 region 1566. NOAA 9 AVHRR GAC data for daytime and nighttime passes were processed for every fifth day from March to July 1985.

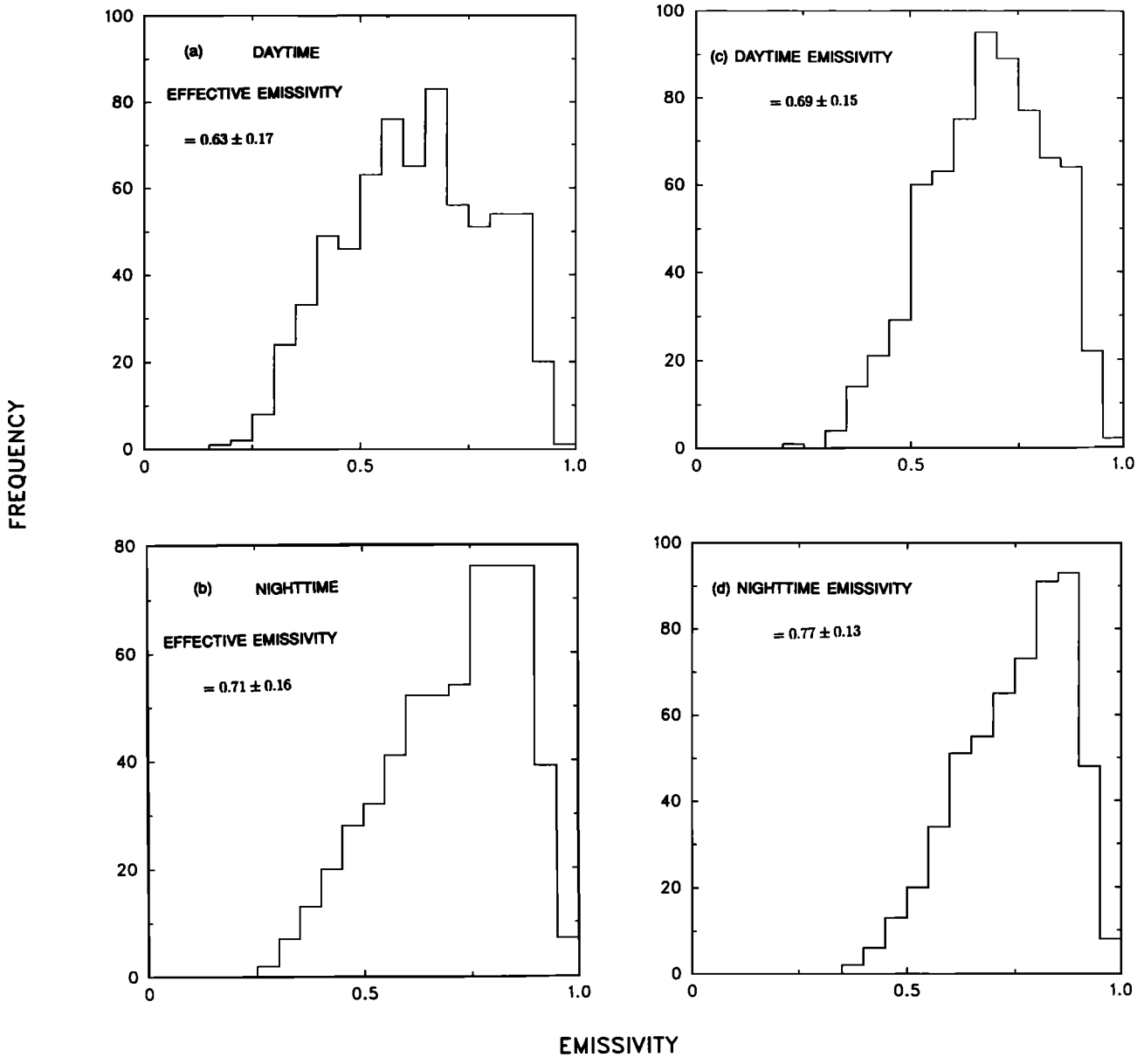

Figure 7. Frequency distribution for 250-km-scale regions of (a) daytime regional-scale effective 11-μm emissivity, (b) nighttime regional-scale effective 11-μm emissivity, (c) daytime regional-scale 11-μm emissivity, and (d) nighttime regional-scale 11-μm emissivity. The effective emissivity is the average of the pixel-scale emissivity weighted by the corresponding pixel-scale cloud cover. The values given in the figures are the means and standard deviations for the 250-km-scale regions.

ranging from 2 to 20 μm with an increment of 0.5 μm. The lower limit of this range was chosen because it falls below the droplet sizes typically found in marine stratocumulus [*Nakajima et al.*, 1991]. The upper limit, as was noted in the previous section, is the limit at which the envelope for the 11- to 12-μm radiance domain collapses to a straight line. Root-mean-square differences between the observed 12-μm radiances for the pixels representing the fifth percentiles in the 10 11-μm radiance intervals and that obtained from the radiative transfer model for the interval were obtained for each effective droplet radius. Each group of root-mean-square differences had a single minimum, like that shown in Figure 5. The effective droplet radius R_{eff} was taken to be that which gave the minimum RMS difference between observed and calculated radiances. Once the effective droplet radius was retrieved, the radiative transfer model was used to obtain the pixel-scale fractional cloud cover and 11-μm emissivity. The sensitivity of the retrieved results to the size of the increment in effective radius used in the adjustment is discussed in the next section.

Points having higher 11- and 12-μm emissions than that associated with the cloud-free pixels were taken to be cloud-free. Emissivity is not defined for these points. Points having lower 11-μm emissions than that associated with the overcast pixels and having 12-μm emissions above the values obtained by extrapolating the straight line associated with the cloud-free and overcast pixels were taken to be overcast and opaque and were therefore given unit cloud

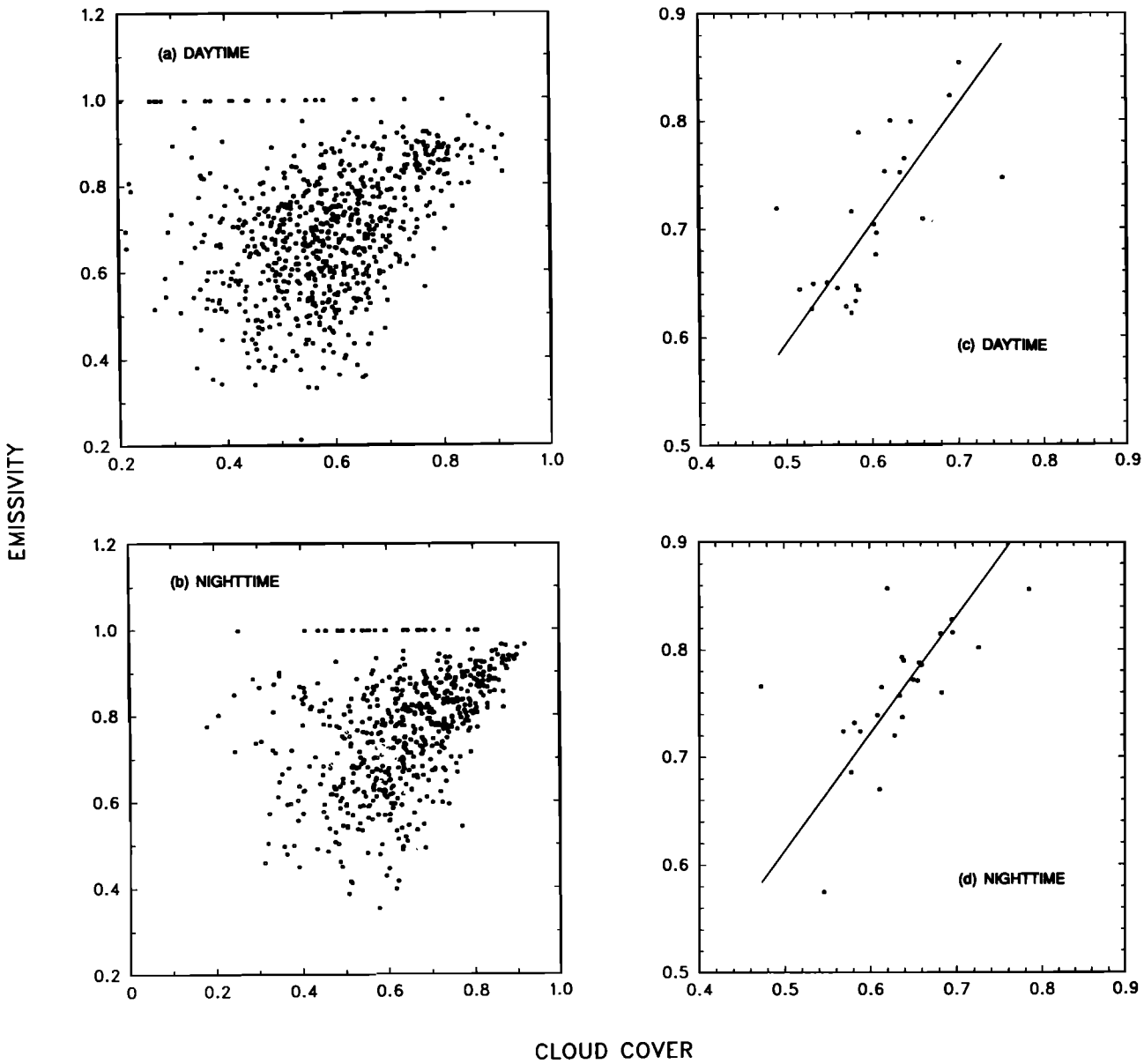

Figure 8. The 11-μm emissivity and fractional cloud cover for (a) daytime and (b) nighttime 250-km-scale regions and for (c) daytime and (d) nighttime least squares fits based on the averages obtained for each day.

cover and unit emissivity. If (1) were applied to calculate the cloud cover associated with pixels having 11- and 12-μm emissions larger than that given by the mean of the cloud-free pixels as determined by the spatial coherence method, it would produce small but negative cloud fractions. Likewise, if (1) were applied to calculate the cloud cover for the pixels having 11- and 12-μm radiances below the mean associated with the overcast pixels as determined by the spatial coherence method, it would produce cloud cover fractions slightly greater than unity. We accept these inconsistencies as errors in the retrieved cloud cover fraction. The sensitivity of the fractional cloud cover and 11-μm emissivity to variations in the emitted radiances associated with the overcast and cloud-free pixels is discussed in the next section. In the same spirit, points having 12-μm emission falling above the values given by the straight line were taken to be opaque broken clouds. They were given unit 11-μm emissivity, and the fractional cloud cover was obtained by applying (1). The points beneath the curve associated with pixels that are overcast by semitransparent cloud were taken to be overcast and were given the emissivity given by the extrapolation of the lines of constant emissivity. Points having 12-μm radiances falling below the line associated with pixels overcast by semitransparent cloud and within the extrapolated lines associated with emissivities equal to zero (vertical line extending from the cloud-free radiances) and 0.05 were treated separately. Because the departures of the 11- and 12-μm radiances from the cloud-free radiances were small, the retrieved emissivity and fractional cloud cover for these pixels were highly uncertain. Here we take the emissivity for the clouds to be 0.025 and the fractional cloud cover to be unity. The results obtained using this assignment are compared below with those obtained for the fractional cloud cover set to zero. These extremes lead to maximum and

minimum values for the retrieved regional-scale fractional cloud cover and emissivity.

Of course, the retrieved products, which in turn are governed by the retrieved effective droplet radius, should be insensitive to the choice of channel (11 or 12 μm) used as the independent variable in fitting the results of the radiative transfer model to the observations. As a check, the roles of the 11- and 12-μm radiances were reversed. As is shown in Figure 5, there was practically no difference in the retrieved effective radius. Typically, the effective radii retrieved by reversing the roles of 11- and 12-μm radiances were within 1 μm of each other.

The regional-scale fractional cloud cover is obtained by averaging the pixel-scale cloud cover derived from the radiative transfer interpretation of the associated 11- and 12-μm radiance pair. In addition, two emissivities were

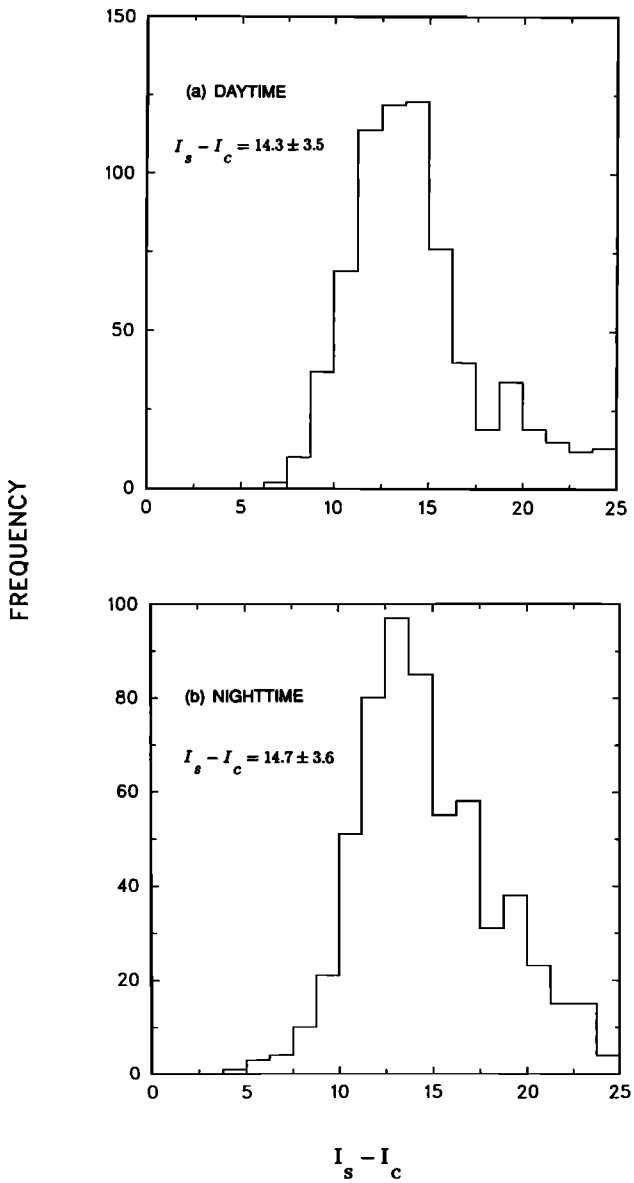

Figure 9. Frequency distribution of the difference between cloud-free and overcast, opaque cloud 11-μm emissions for 250-km-scale regions: (a) daytime; (b) nighttime.

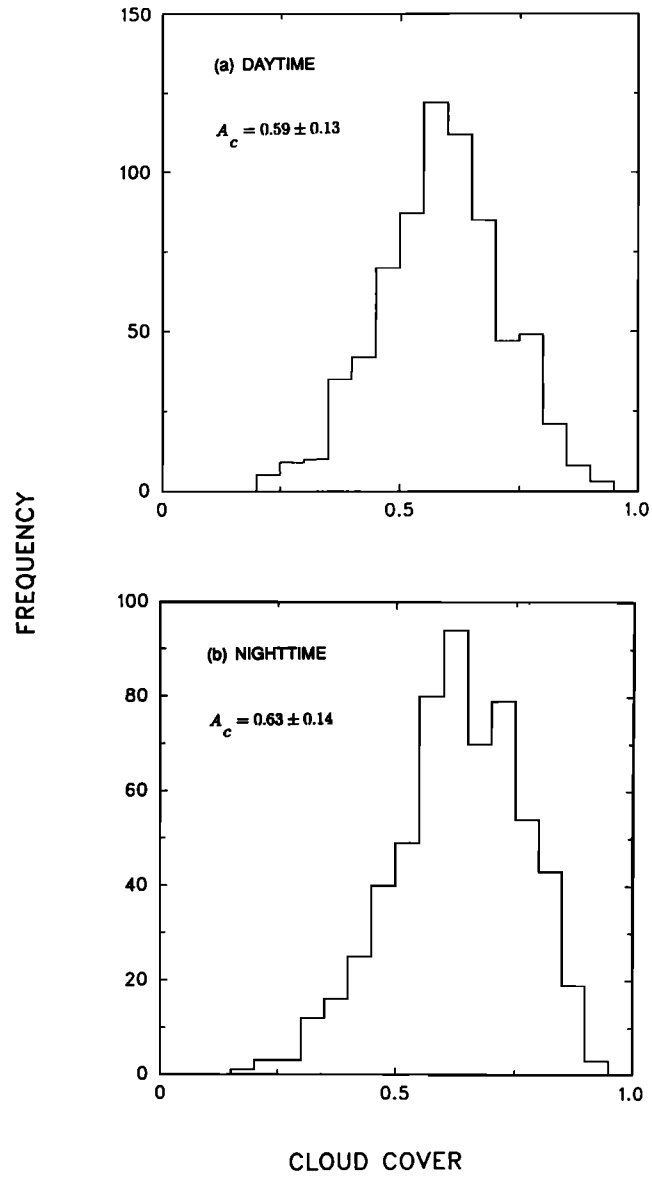

Figure 10. Frequency distribution of fractional cloud cover for 250-km regions: (a) daytime; (b) nighttime.

calculated. The first is representative of the emissivity for a typical cloud. It is obtained by averaging the pixel-scale 11-μm emissivities. The second is the emissivity used in conjunction with the regional-scale cloud cover to produce the regional mean emitted radiance. We call this emissivity the "effective emissivity." It is obtained by averaging the pixel-scale emissivity weighted by the corresponding pixel-scale fractional cloud cover.

4. Sensitivity Studies

Sensitivity studies were performed to determine the uncertainties in regional-scale fractional cloud cover and 11-μm emissivity caused by uncertainties in the retrieved effective droplet radius, in the emission associated with pixels that were cloud-free, and in the emission associated with pixels that were overcast by opaque cloud. The standard deviations of the radiances associated with the pixels

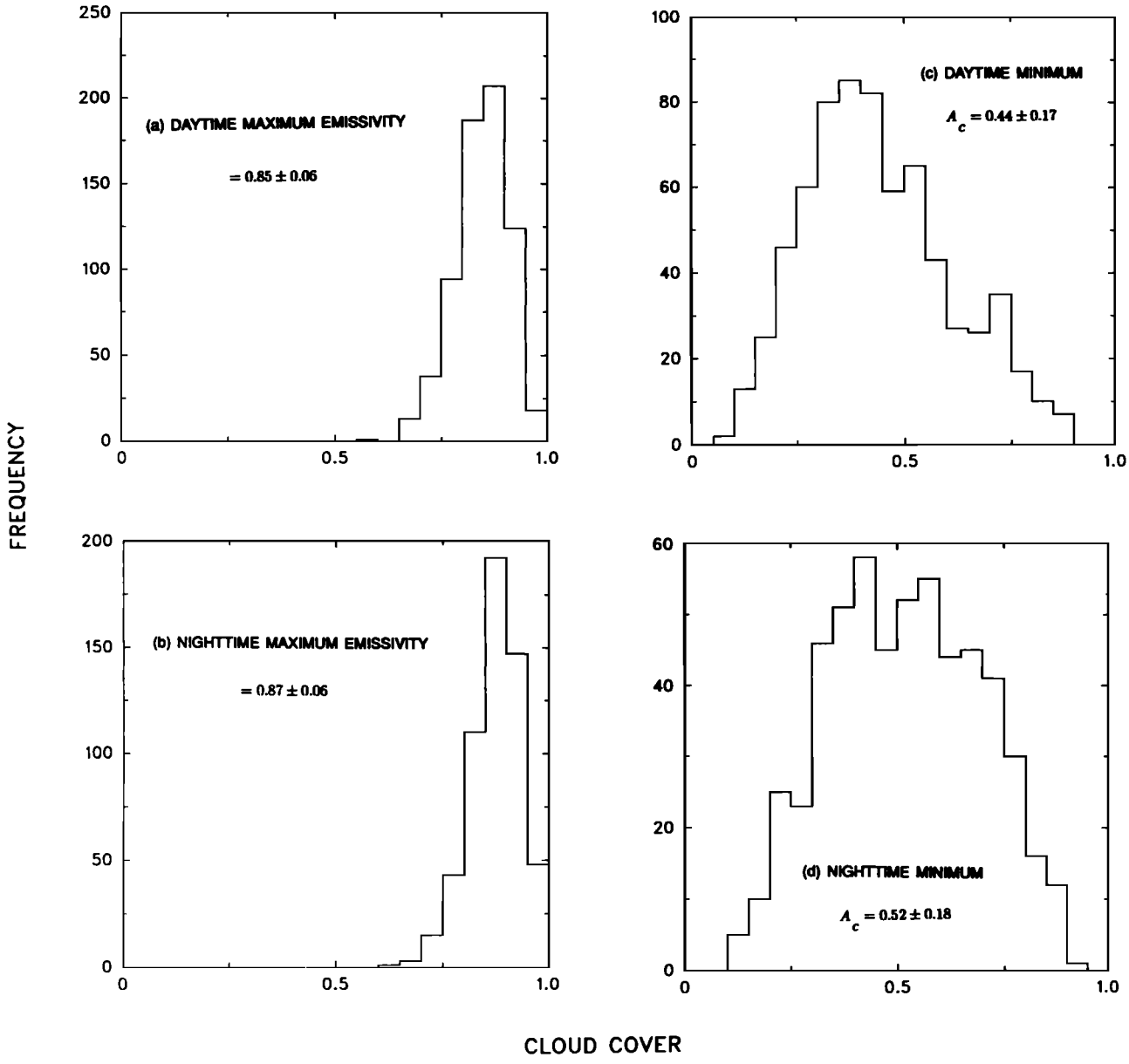

Figure 11. Frequency distribution of maximum estimates for (a) daytime and (b) nighttime 11-μm emissivities for 250-km regions obtained by setting the pixel-scale fractional cloud cover to zero for pixels having emissivities of <0.05 and of corresponding minimum estimates for (c) daytime and (d) nighttime fractional cloud covers.

that were cloud-free and overcast as determined by the spatial coherence method were used for the uncertainties of the cloud-free and overcast, opaque cloud radiances. The sensitivities of regional-scale fractional cloud cover, 11-μm emissivity, and effective droplet radius to changes in the emission associated with the cloud-free and overcast, opaque cloud pixels were determined by calculating variations in the retrieved parameters obtained by varying the cloud-free and overcast, opaque cloud radiances 1 standard deviation above and below their mean values. The maximum variation in fractional cloud cover for the ensemble of daytime and nighttime cases studied here was $|\Delta A_c| = 0.06$, for the 11-μm emissivity the maximum variation was $|\Delta\varepsilon| = 0.07$, and for the effective droplet radius the maximum variation was $|\Delta R_{\text{eff}}| = 1.7$ μm.

In addition, the retrieved droplet radius was altered by ±0.5 μm, the increment used in the procedure to obtain the best fit to the 11- to 12-μm radiance domain occupied by the pixel-scale radiances. The changes in regional-scale fractional cloud cover and 11-μm emissivity were found to vary by less than ±0.01.

The range of effective droplet radius spanned in the retrieval process was 2–20 μm. Clouds in regions for which the effective droplet radius was found to be larger than 20 μm were treated as if they were opaque. This procedure gives rise to a discontinuity in the distribution of cloud

emissivity. Whenever the effective radius was found to be smaller than 20 μm, some pixels were found to have emissivities less than unity regardless of how linear the 11- to 12-μm scatterplot appeared. On the other hand, whenever the effective droplet radius was found to be larger than 20 μm, all pixels were found to have unit emissivities. Because of this discontinuity, the fitting process was repeated to investigate the sensitivity of the retrieved results to the value of the maximum effective droplet radius. The ending effective droplet radii were taken to be 15 and 25 μm. For the ensemble studied here, the change in retrieved emissivity was within 0.02 for both the 15- and the 25-μm cases, and the change in the retrieved fractional cloud cover was zero.

Finally, as noted by *Lin and Coakley* [1993], the retrieved products are sensitive to the spatial resolution of the imager. The procedure requires that somewhere in the region being analyzed there be pixels which are overcast by semitransparent cloud. These pixels give rise to the lower envelope of the 11- to 12-μm scatterplot. To test whether this condition was met for the ensemble of cases studied here, the spatial resolution of the observations was degraded and the shifts in the retrieved products were noted. Degrading the spatial resolution of the observations from 4 to 8 km shifted the regional-scale fractional cloud cover +0.01, the 11-μm emissivity −0.04, and the effective droplet radius +2 μm. These values probably underestimate the actual bias. Better estimates of the bias might be obtained through the analysis of observations capable of resolving the typical spatial variability of the radiation field for marine stratocumulus, like the Landsat data analyzed by *Wielicki and Parker* [1992].

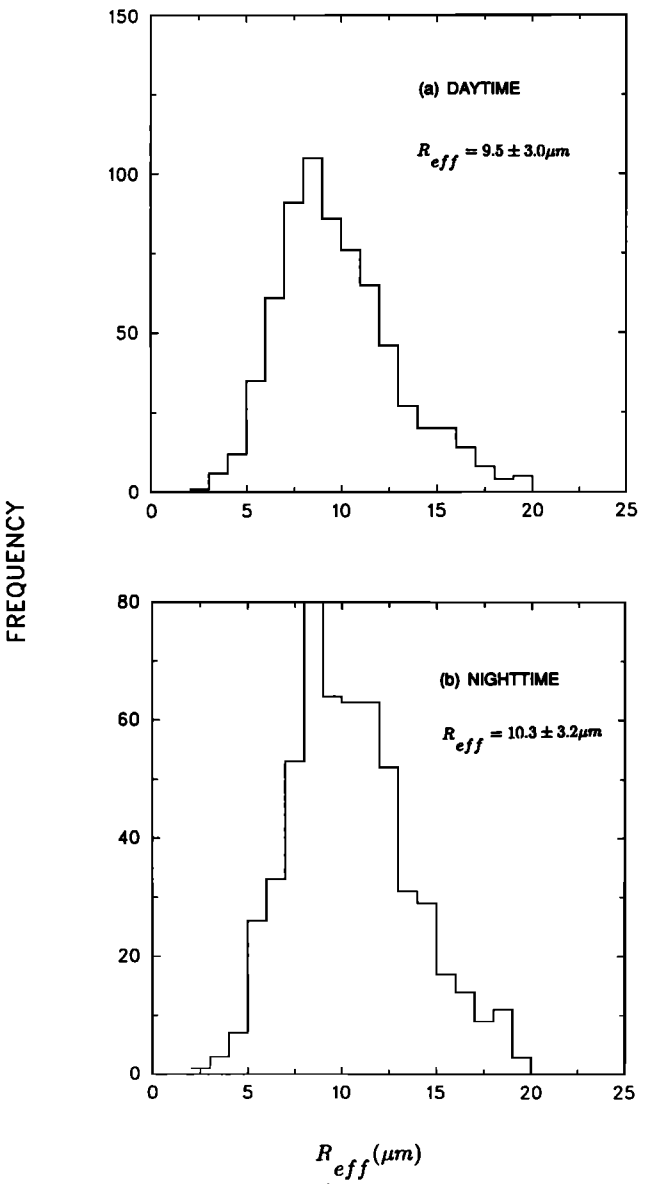

Figure 12. Frequency distribution of effective droplet radius for 250-km-scale regions: (a) daytime; (b) nighttime.

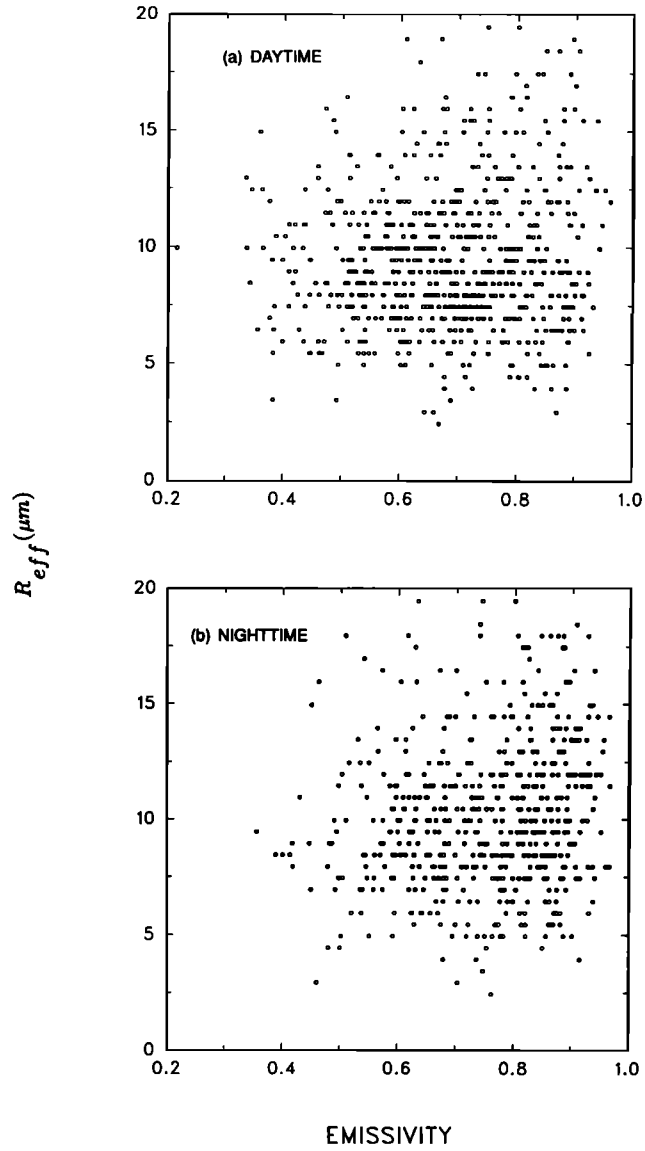

Figure 13. Emissivity and effective droplet radius for 250-km-scale regions: (a) daytime; (b) nighttime.

5. Data Analysis and Results

Daytime and nighttime 4-km NOAA 9 AVHRR global area coverage (GAC) observations were analyzed for a region off the coast of Chile as shown in Figure 6. The observations

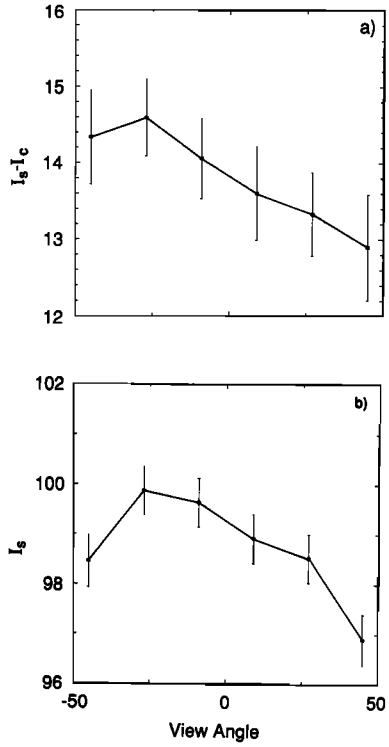

Figure 14. Viewing angle dependence of (a) difference between cloud-free and overcast, opaque cloud 11-μm radiances (mW m^{-2} sr^{-1} cm) and (b) cloud-free 11-μm radiances. Negative viewing angles are associated with the western portion of the scan, away from the South American continent.

were sampled every 5 or 6 days from March through July 1985. The data were part of the Earth Radiation Budget Experiment (ERBE) Scene Identification Validation (V-5) data product. There were six daytime and six nighttime orbital segments for each month. The data for each orbital segment were divided into four scenes, with each scene containing a 384 × 256 scan spot × scan line array of pixels. Each scene was further divided into 24 frames. Each frame was a 64 × 64 scan spot × scan line array of pixels. The model fits were applied only to frames for which there was a single-layered system of broken low-level clouds. A single layer was presumed to be present if all of the overcast pixels in the frame were found to be part of only one layer as deduced by the spatial coherence method [*Coakley and Baldwin*, 1984]. Furthermore, the mean of the 11-μm radiances associated with the overcast pixels I_c and the standard deviation ΔI_c explained the 10th percentile I_{10} of the 11-μm radiances for the region. This condition was assumed to be met when

$$I_{10} > I_c - 2\Delta I_c. \tag{2}$$

Identical procedures were used in previous studies to identify single-layered cloud systems [*Coakley and Davies*, 1986; *Coakley*, 1991]. In addition, only 250-km frame scale regions which contained both cloud-free and overcast pixels were analyzed. The presence of both cloud-free and overcast pixels ensured that the region was neither overcast nor cloud-free. Finally, only observations with low-level clouds were analyzed. Low-level clouds were presumed to be present whenever the difference between the 11-μm radiances associated with overcast and cloud-free pixels I_s satisfied the condition

$$I_s - I_c \leq 25 \text{ mW m}^{-2} \text{ sr}^{-1} \text{ cm}. \tag{3}$$

At 11-μm the radiances for blackbodies at 290° and 273°K differ by about 25 mW m^{-2} sr^{-1} cm.

In the 5-month period studied, over 2500 frames of daytime data were analyzed. Of these, over 1800 contained either upper level clouds or multilayered clouds, were either overcast or cloud-free, or had a single-layered low-level cloud system, but nowhere in the region were there cloud-free or overcast pixels. Such frames were judged to be unsuitable for the present study. The number of frames containing single-layered, broken, low-level cloud and both overcast and cloud-free pixels was 710 (27%). For the nighttime passes, almost 2700 frames were available for analysis. Of these, 2100 contained either upper level or

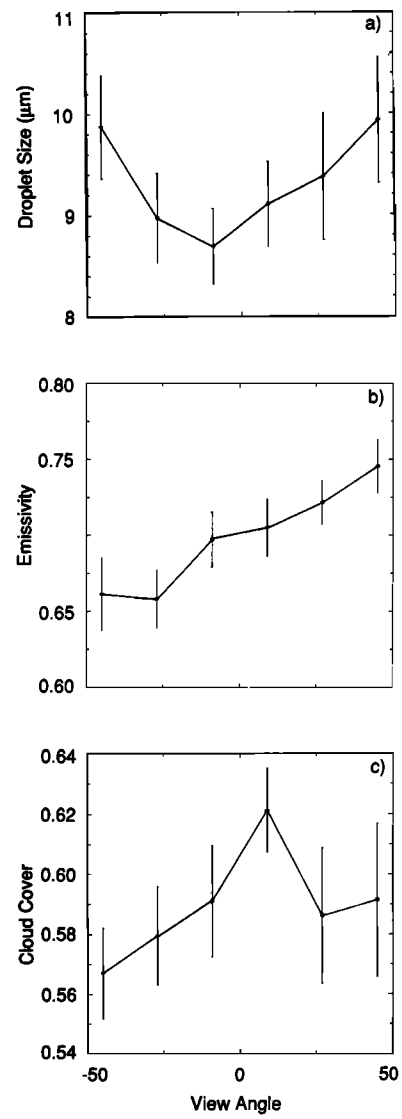

Figure 15. Viewing angle dependence of (a) retrieved effective droplet radius, (b) 11-μm emissivity, and (c) fractional cloud cover.

multilayered clouds, were overcast or cloud-free, or had a single-layered low-level cloud system, but nowhere in the region were there cloud-free or overcast pixels. Of these, 611 (22%) contained single-layered, broken, low-level cloud systems with both cloud-free and overcast pixels and were thus suitable for this study.

Figure 7 shows the 250-km frame scale frequency distribution of 11-μm emissivities. The values for the cloud-weighted effective emissivity were 0.65 ± 0.02 for daytime observations and 0.68 ± 0.02 for nighttime observations; those for the emissivity were 0.70 ± 0.01 for daytime observations and 0.76 ± 0.01 for nighttime observations. The values given here (and subsequently) are the averages of daily mean values and the estimated standard deviations for the mean values. The daily means were obtained by averaging the frame scale emissivities for each day. The standard deviations of the means were obtained from the standard deviation of the daily means assuming that observations on different days were statistically independent. The means and standard deviations given in the figures (and in subsequent figures) are those for the ensemble of 250-km frames. Clearly, a substantial fraction of marine stratocumulus was semitransparent at 11 μm.

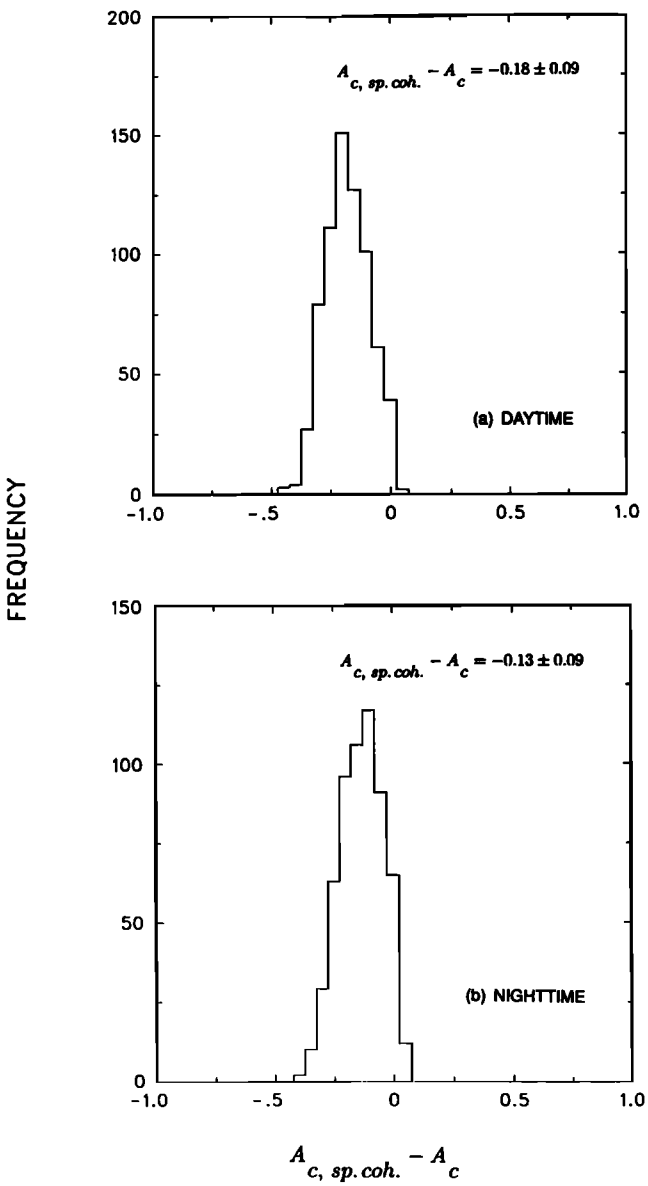

Figure 16. Frequency distribution of difference between spatial coherence derived cloud cover and 11- and 12-μm-derived cloud cover for 250-km-scale regions: (*a*) daytime; (*b*) nighttime.

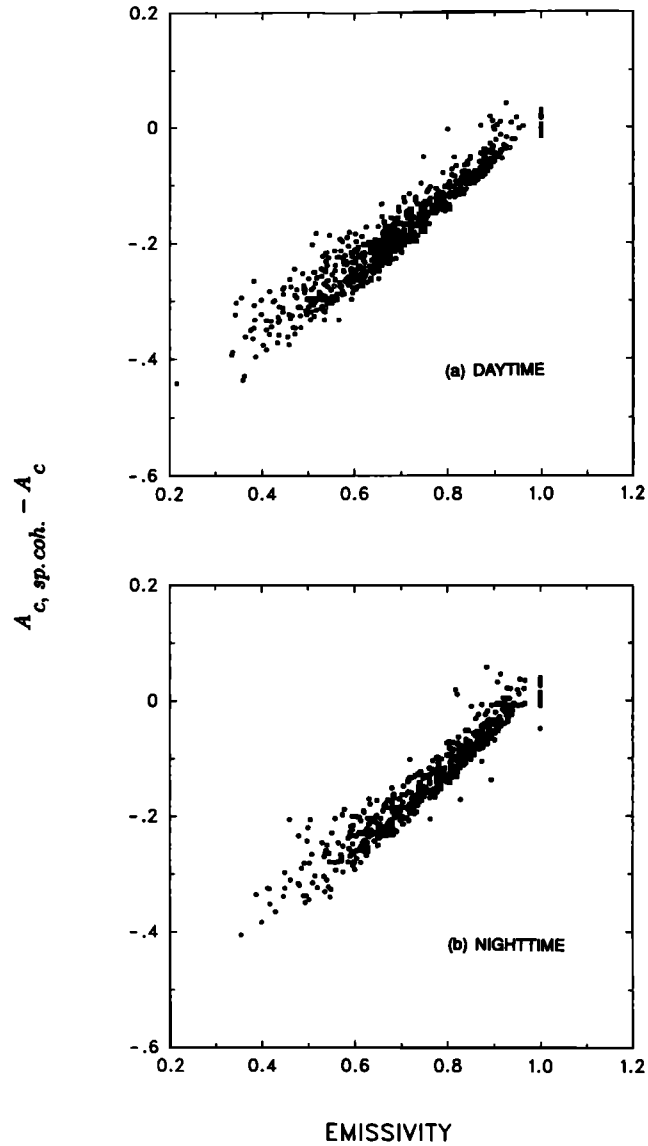

Figure 17. Emissivity and difference between spatial coherence and 11- and 12-μm-derived fractional cloud cover for 250-km-scale regions: (a) daytime; (b) nighttime.

The results shown in Figure 7 indicate that there was a small difference between daytime and nighttime emissivities. The difference is, however, partly due to the change in cloud cover. A strong correlation was found between the regional-scale 11-μm emissivity and the fractional cloud cover, as is shown in Figure 8. For the 27 daytime and 28 nighttime average values of emissivity and fractional cloud cover, the correlation between 11-μm emissivity and fractional cloud cover was given by

$$\varepsilon = (1.10 \pm 0.08)A_c + (0.05 \pm 0.05) \quad (4)$$

for the daytime observations and

$$\varepsilon = (1.08 \pm 0.08)A_c + (0.07 \pm 0.05) \quad (5)$$

for the nighttime observations. These relationships and the means for the daytime 0.60 ± 0.01 and nighttime 0.63 ± 0.01 fractional cloud covers lead to the conclusion that about half of the daytime-nighttime difference in emissivity was explained by the change in cloud cover. The remainder of the difference was presumably due to an increase in cloud liquid water such as might accompany an increase in cloud thickness.

In addition to the strong correlation between emissivity and fractional cloud cover, Figure 8 also shows the discontinuity in the 11-μm emissivity mentioned in the previous section. The ability to distinguish between pixels containing opaque, broken clouds having droplets of any size and those containing semitransparent clouds having large droplets is impossible once $R_{\text{eff}} > 20$ μm. When either condition applies, the envelope illustrated in Figure 2 collapses to a straight line. Because we constrained the retrieved $R_{\text{eff}} \leq 20$ μm, the regional-scale emissivity exhibits a discontinuity as a distinct separation between cases for which $\varepsilon = 1$ and $\varepsilon < 1$. Whether the radiances for the cases having $\varepsilon = 1$ were due to semitransparent clouds having large droplets or to broken opaque clouds, few cases exhibited the collapse of the envelope in the 11- to 12-μm radiance domain to a straight line. That is, the majority of 250-km-scale frames containing broken marine stratocumulus exhibited radiance signatures indicating the presence of clouds that were semitransparent at 11 μm.

We suspect that the correlation between emissivity and fractional cloud cover shown in Figure 8 indicates that clouds thin at their edges, thereby giving rise to a semitransparent component. This inference is deduced in part from the observation that when the regional-scale cloud cover is small, then the cloud cover in pixels containing broken clouds is also, on average, small [*Chang and Coakley*, 1993]. Consequently, the ratio of cloud edge material to the total fractional cloud cover increases as the regional fractional cloud cover decreases. So, as the regional-scale cloud cover decreases, the relative contribution from cloud material that is semitransparent increases. This view is consistent with the model for layered clouds proposed in earlier studies [*Coakley and Davies*, 1986; *Coakley*, 1991] and with the analysis of Landsat imagery data [*Wielicki and Parker*, 1992].

Figure 9 shows differences between the cloud-free and overcast 11-μm emissions. These differences were used as an index of cloud height. Larger differences were taken to indicate higher clouds. The figure shows no significant difference between daytime and nighttime observations.

Figure 10 shows the distribution of fractional cloud cover for daytime and nighttime observations. The average fractional cloud cover for the nighttime observations, 0.63 ± 0.01, is significantly higher than that for the daytime observations, 0.60 ± 0.01. It should be noted that here we have included only 250-km frames which contained broken, single-layered, low-level clouds. The fraction of frames overcast at night by low-level layered clouds is also higher than during the day. The fraction overcast is, however, small (<5%).

The average 11-μm emissivities shown in Figure 7 were obtained by setting the fractional cloud cover for the pixels having $\varepsilon < 0.05$ to unity, as was described in section 3. On average, the number of such pixels was 10–15% of the total number of pixels in a region. To assess the impact of these pixels, results were obtained for cases in which their fractional cloud cover was set to zero. Doing so yields maximum values for the 11-μm emissivities and minimum values for the cloud cover fractions on the 250-km scale. Figure 11 shows the maximum emissivities and the minimum fractional cloud cover obtained by setting $A_c = 0$ for these pixels. The effect of the low-emissivity pixels is sizable. Taking the difference between maximum and minimum estimates to represent 3 standard deviations, as is approximately the relationship between the standard deviation and the extrema for uniform distributions, the estimated (1-sigma) uncertainties in the retrieved emissivity are 0.05 for daytime observations and 0.04 for nighttime observations. The results give estimated (1-sigma) uncertainties in the fractional cloud cover of 0.05 for daytime observations and 0.04 for nighttime observations.

The distribution of effective droplet radius is shown in Figure 12. The average effective radius was around 10 μm. This value falls in the range of values obtained by *Nakajima et al.* [1991] for the First ISCCP Regional Experiment (FIRE) Marine Stratocumulus Intensive Field Observations off the coast of California in July 1987. The effective droplet radii were 9.3 μm for daytime observations and 10.2 μm for nighttime observations. The standard deviation of the mean effective droplet radius was estimated to be 0.3 μm, so the nighttime value was significantly higher than the daytime value. *Minnis et al.* [1992] deduced from a combination of visible and infrared imagery data and microwave radiometer data that droplet radius in the midafternoon was typically smaller than that at sunrise for the 1987 FIRE Intensive Field Observations off the coast of California.

Figure 12 shows that there were few regions with effective droplet radii less than 4 μm. Thus the use of 2 μm as the starting value for the retrieval procedure appears to be justified.

Figure 13 shows the effective droplet radii and 11-μm emissivities retrieved for the 250-km frames. There appears to be little if any correlation between droplet radius and 11-μm emissivity obtained with this analysis.

Because the Eddington approximation used here to perform the radiative transfer calculations does not allow for anisotropy in the calculated emissivities and transmissivities, the retrieved products were examined for dependence on viewing angle. Figure 14 shows the variation with view angle from nadir of the cloud-free 11-μm emission and differences between the cloud-free and overcast, opaque cloud 11-μm radiances. Figure 15 shows the viewing angle dependence of the effective droplet radius, 11-μm emissivity, and fractional cloud cover. The points give the averages of the overpass means, and the error bars give the estimated standard deviations of the overpass means. The results shown in the figures are for the combination of daytime and nighttime passes. The angular dependence of the variables is small but significant. Some of the dependence may be due to the use of the Eddington approximation, but some, like the emission associated with the cloud-free ocean background, is due to geographical trends in the ensemble. The negative viewing angles were for observations on the side of the scan furthest from the South American coast. Positive viewing angles were for observations on the side nearest the coast.

Finally, the estimated frame scale fractional cloud cover

was compared with that calculated by the spatial coherence method. Figure 16 shows the distribution of the differences (spatial coherence − multispectral infrared retrieval). The spatial coherence method underestimated fractional cloud cover for marine stratocumulus by $\Delta A_c = -0.17$ for daytime observations and by $\Delta A_c = -0.14$ for nighttime observations. The spatial coherence method ignores the semitransparent cloud edges. It assumes that clouds are everywhere opaque. The results reported here are comparable to those reported by *Wielicki and Parker* [1992]. Based on retrievals obtained from 114-m resolution Landsat data, they concluded that the spatial coherence method underestimated fractional cloud cover for marine stratocumulus by $\Delta A_c = -0.18$. Figure 17 shows 11-μm emissivities and differences in the fractional cloud cover retrieved using the current multispectral infrared retrieval and that obtained with the spatial coherence method (spatial coherence − multispectral infrared retrieval). The differences, not surprisingly, are highly correlated with the emissivities.

6. Conclusions

The 11- and 12-μm radiances obtained from 4-km NOAA 9 AVHRR GAC observations were used to derive regional-scale estimates of fractional cloud cover, 11-μm emissivities, and effective droplet radii for single-layered marine stratocumulus systems off the coast of South America. The observations were limited to layers which had breaks within 250-km-scale regions. Such layers constituted 27% of all the 250-km regions contained in the daytime observations and 22% of the nighttime observations. The occurrence of single-layered, low-level clouds which completely covered 250-km regions was rare (<5%).

The retrievals indicated that the average 250-km-scale 11-μm emissivity for broken marine stratocumulus was substantially less than unity: 0.70 for daytime observations and 0.76 for nighttime observations. Because the regional-scale 11-μm emissivity appeared to be correlated with the regional-scale cloud cover and because cloud cover for pixels containing broken clouds is proportional to the regional-scale cloud cover [*Chang and Coakley*, 1993], the low emissivity appears to be due to clouds thinning at the edges. Evidently the edge material is semitransparent at 11 μm, and it constitutes a sizable fraction of the area covered by the cloud. Because of the low emissivity, the spatial coherence method [*Coakley and Bretherton*, 1982], which takes clouds to be opaque at infrared wavelengths, severely underestimated the fractional cloud cover (ΔA_c was −0.17 for daytime observations and −0.14 for nighttime observations). This finding agrees with that of *Wielicki and Parker* [1992], who found a similar bias in spatial coherence retrievals applied to Landsat imagery data.

Cloud cover for broken marine stratocumulus was only slightly (but significantly) higher at night (0.63) than during the day (0.60). The 11-μm emissivity was also slightly higher. About half of the increase, however, was explained by the correlation found between the regional-scale fractional cloud cover and emissivity coupled with the increase in cloud cover for the nighttime observations. This portion of the day-to-night increase in regional-scale 11-μm emissivity was taken to be due to a reduction in the relative area occupied by cloud edge material. In addition, there appeared to be no change in the difference between emission from pixels overcast by opaque clouds and cloud-free pixels for daytime and nighttime observations, indicating no difference in cloud height. The effective droplet radius was slightly (but significantly) higher at night (10.2 μm) than during the day (9.3 μm).

As noted by *Lin and Coakley* [1993], the retrieved quantities are subject to several ambiguities which can be resolved only through comparison of cloud physical properties obtained through alternate methods, such as independent retrievals using radiances at 0.63 and 3.7 μm, the other spectral channels provided by AVHRR observations. Despite these ambiguities, the sensitivity studies performed here revealed that only a few broken marine stratocumulus layers at the 250-km scale exhibited behavior that would be expected were the clouds opaque at 11 μm. The vast majority behaved as if their 11-μm emissivities were substantially less than unity.

Acknowledgments. This work was supported in part by the National Science Foundation through grant ATM-8912669 and through grants from the Office of Naval Research and the Western regional office of the National Institute for Global Environmental Change. The NASA ERBE provided the V-5 data which made this study possible.

References

Arking, A., and J. D. Childs, Retrieval of cloud cover parameters from multispectral satellite images, *J. Clim. Appl. Meteorol.*, *24*, 322–333, 1985.

Chang, F.-L., and J. A. Coakley, Jr., Estimating errors in fractional cloud cover obtained with infrared threshold methods, *J. Geophys. Res.*, *98*, 8825–8839, 1993.

Coakley, J. A., Jr., Properties of multi-layered cloud systems from satellite imagery, *J. Geophys. Res.*, *88*, 10,818–10,828, 1983.

Coakley, J. A., Jr., Reflectivities of uniform and broken layered clouds, *Tellus*, *43B*, 420–443, 1991.

Coakley, J. A., Jr., and D. G. Baldwin, Towards the objective analysis of clouds from satellite imagery data, *J. Clim. Appl. Meteorol.*, *23*, 1065–1099, 1984.

Coakley, J. A., Jr., and F. P. Bretherton, Cloud cover from high-resolution scanner data: Detecting and allowing for partially filled fields of view, *J. Geophys. Res.*, *87*, 4917–4932, 1982.

Coakley, J. A., Jr., and R. Davies, The effect of cloud sides on reflected solar radiation as deduced from satellite observations, *J. Atmos. Sci.*, *43*, 1025–1035, 1986.

Goody, R. M., and Y. L. Yung, *Atmospheric Radiation Theoretical Basis*, Oxford University Press, New York, 1989.

Lin, X., and J. A. Coakley, Jr., Retrieval of properties for semitransparent clouds from multispectral infrared imagery data, *J. Geophys. Res.*, *98*, 18,501–18,514, 1993.

Minnis, P., and E. F. Harrison, Diurnal variability of regional cloud and clear-sky radiative parameters derived from GOES data, II, November 1978 cloud distributions, *J. Clim. Appl. Meteorol.*, *23*, 1021–1031, 1984.

Minnis, P., P. W. Heck, D. F. Young, C. W. Fairall, and J. B. Snider, Stratocumulus cloud properties derived from simultaneous satellite and island-based instrumentation during FIRE, *J. Appl. Meteorol.*, *31*, 317–339, 1992.

Molnar, G., and J. A. Coakley, Jr., The retrieval of cloud cover from satellite imagery data: A statistical approach, *J. Geophys. Res.*, *90*, 12,960–12,970, 1985.

Nakajima, T., and M. D. King, Determination of the optical thickness and effective particle radius of clouds from reflected solar radiation measurements, I, Theory, *J. Atmos. Sci.*, *47*, 1878–1893, 1990.

Nakajima, T., M. D. King, J. D. Spinhirne, and L. F. Radke, Determination of the optical thickness and effective particle radius of clouds from reflected solar radiation measurements, II,

Marine stratocumulus observations, *J. Atmos. Sci.*, *48*, 728–750, 1991.

Platt, C. M. R., On the bispectral method for cloud parameter determination from satellite VISSIR data: Separating broken and semitransparent cloud, *J. Clim. Appl. Meteorol.*, *22*, 429–439, 1983.

Rossow, W. B., et al., ISCCP cloud algorithm intercomparison, *J. Clim. Appl. Meteorol.*, *24*, 877–903, 1985.

Wielicki, B. A., and L. Parker, On the determination of cloud cover from satellite sensors: The effect of sensor spatial resolution, *J. Geophys. Res.*, *97*, 12,799–12,823, 1992.

J. A. Coakley, Jr., and X. Lin, College of Oceanic and Atmospheric Sciences, Oregon State University, Corvallis, OR 97331-2209.

G. Luo, UCAR Visiting Scientist Program, NOAA/NESDIS, Washington, Camp Springs, MD 20746.

(Received August 22, 1992; revised August 26, 1993; accepted August 26, 1993.)